J Mater Sci (2008) 43:6539–6545
DOI 10.1007/s10853-008-2818-4

Photoluminescent properties of ZnS:Mn nanoparticles with in-built surfactant

Zinki Jindal · N. K. Verma

Received: 3 January 2008 / Accepted: 18 June 2008 / Published online: 8 July 2008

Abstract Mn-doped ZnS nanoparticles, having average diameter 3–5 nm, have been synthesized using chemical precipitation technique without using any external capping agent. Zinc blende crystal structure has been confirmed using the X-ray diffraction studies. The effect of various concentrations of Mn doping on the photoluminescent properties of ZnS nanoparticles has been studied. The time-resolved photoluminescence spectra of the ZnS:Mn quantum dots have been recorded and various parameters like lifetimes, trap depths, and decay constant have been calculated from the decay curves at room temperature. The band gap was calculated using UV–Visible absorption spectra.

Introduction

In recent years, research involving Mn-doped nanocrystalline ZnS (ZnS:Mn) has grown extensively, mainly due to the high quantum luminescence efficiencies that have been reported [1, 2]. ZnS is an important and one among the oldest member of the family of wide-gap (3.66 eV, at room temperature) semiconductors and probably the most important material used as phosphor host [3]. Due to unique optical properties and potential applications, doped semiconductor nanocrystals have attracted extensive research interests [4]. This II–VI compound semiconductors have been studied for a variety of applications such as optical coatings, photoconductors, optic modulators, electro-optic modulators, flat panel displays, electroluminescent devices, sensors, and lasers, and also have been applied in photocatalyst, infrared windows, pigments, and nonlinear optical devices [5, 6]. Numerous researchers have investigated the structural and luminescent properties of doped phosphor nanoparticles, especially Mn^{2+}-doped ZnS nanocrystals, as ZnS can be doped with Mn very easily [7]. This doping causes a visible orange luminescence at about 585 nm. It is well known that ZnS doped with Mn exhibits attractive light-emitting properties with increased optically active sites for applications as efficient phosphors [8]. These nanomaterials behave differently from bulk semiconductors as they are influenced by various surface states arising due to quantum confinement effect and large surface-to-volume ratio. ZnS nanoparticles have been mostly synthesized with methods like inverse micelle [9], zeolite [10], or vapor-phase condensation method [11], but have certain problems such as low powder collection and complex processing procedures. Chemical precipitation method is better than other techniques for producing efficiently luminescent nanophosphors in terms of process simplicity, effectiveness of doping, higher yield and has a very simple procedure with low-cost apparatus [12].

The increase in particle size increases surface energy resulting in agglomeration of the particles. To control the size of the semiconductor nanoparticles, numerous researchers have used the capping agent [12]. But if surfactant or capping agent is used to confine particles, then it becomes difficult to completely washout the surfactant molecules from the surface of the nanoparticles, so unintentional defect layers could be introduced in the product, and, therefore it is always desirable to develop technique to synthesize nanoparticles without any capping agent. In the present work, Mn^{2+}-doped ZnS nanoparticles have been synthesized by the chemical precipitation method in an

Z. Jindal (✉) · N. K. Verma
School of Physics & Materials Science, Thapar University, Patiala 147004, India
e-mail: zinkijindal@thapar.edu; zinkijindal@gmail.com

aqueous media at room temperature without using any external capping agent. The nanoparticles, thus obtained, were studied for their optical absorption, energy- and time-resolved photoluminescence, in an attempt, to see the effect of Mn^{2+} doping in ZnS.

Experimental

For the synthesis of ZnS:Mn nanoparticles, 0.5 M zinc acetate (aqueous media) solution was mixed with varying concentrations (0–15 at.%) of manganese acetate solution with constant magnetic stirring. Then 0.5 M Na_2S solution was added to the mixture and a colloidal suspension was obtained immediately after adding Na_2S solution. These analytic grade chemicals have been purchased from sd-fine Chemicals, India. The solution was centrifuged and the precipitates were filtered and washed several times using distilled water. Then the product was dried in vacuum oven at a temperature of about 60 °C. The dried flakes were crushed in a pestle-mortar till a very fine powder was obtained. This powder was collected in airtight containers and was used for all measurements.

Characterizations

The undoped and doped ZnS nanoparticles were characterized using D/max Rint 2000 Rigaku (Tokyo) X-ray diffraction machine using copper characteristic wavelength of 1.54 Å (Hitachi; S-2300). Microstructure and crystal structures of the products were further studied through a high-resolution transmission electron microscope (HRTEM; JEOL 2010). For TEM study a colloidal suspension of nanoparticles in ethanol was prepared by ultrasonic treatment and then deposited on carbon-coated copper grid. The surface chemistry of the samples was analyzed with Fourier Transform Infrared Spectroscopy (FTIR). The samples were mixed with anhydrous KBr and pressed into a pellet for FTIR. FTIR was performed with a Perkin Elmer spectrometer Spectrum RX-I (at a resolution of 2 cm^{-1}). Photoluminescence (PL) measurements were carried out at room temperature with a luminescence spectrometer (Hitachi, FL 2500) using 325 nm as the excitation optical absorbance was recorded by a spectrophotometer (Hitachi; U-3410). The luminescent time decay set-up consisted of a pulsed laser, a photosensor set-up, and a digital oscilloscope interfaced with a computer. A high peak power (10 kW), pulsed (<10 ns) N_2-Laser (337.1 nm), was used as an excitation source. The angle between excitation and detection paths was 90° and the optical filter was used to remove the scattered light. The resulting photoluminescence was detected using a photomultiplier (RCA 8053 PMT) and a digital storage oscilloscope (Tektronix TDS 1012) monitored the photoluminescence decay. The data was then stored in the computer for further analysis. Time-resolved photoluminescence spectroscopy was carried out for lifetime, trap depth, and decay constant measurements. UV–Visible absorption spectra were recorded by dispersing the nanoparticles in spectroscopic grade ethanol, using a spectrophotometer (Hitachi U 3410).

Results and discussion

Figure 1 shows the X-ray diffraction (XRD) patterns for ZnS nanocrystallites, which indicate that all the samples are of zinc blende (cubic) structure. Diffraction peaks from (111), (220), and (311) planes have only appeared in XRD patterns and all other high-angle peaks have submerged in the background due to the large line broadening, which is attributed to nanosize of the particles. The average size of the nanoparticles was estimated from the line broadening of the XRD peaks using the Scherrer's equation [13]

$$d = \frac{0.89\lambda}{\beta \cos \theta_B} \quad (1)$$

where d is the average diameter of the nanoparticles, λ is the wavelength of CuKα (1.541 Å) radiation, β (in radians) is the full width at half maximum (FWHM), and θ_B is the Bragg angle. The average particle size, calculated using

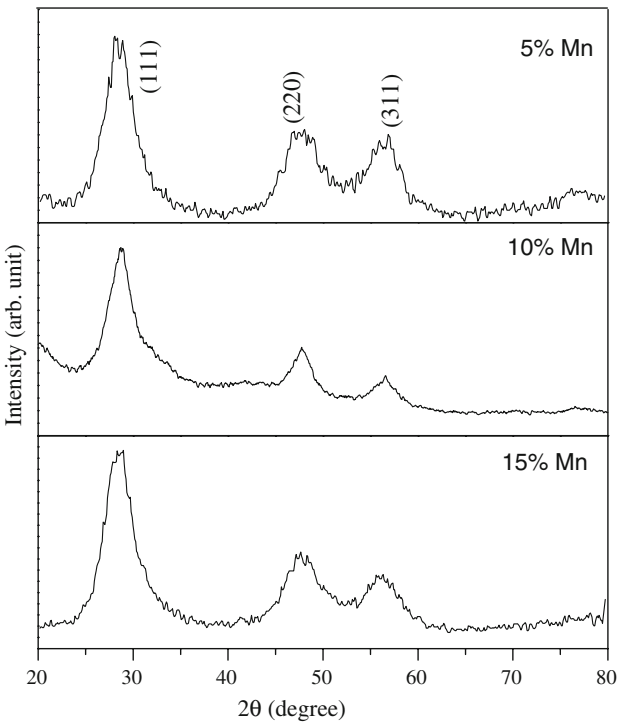

Fig. 1 XRD pattern of Mn^{2+}-doped ZnS nanoparticles (average particle size ~2 nm calculated from peak broadening)

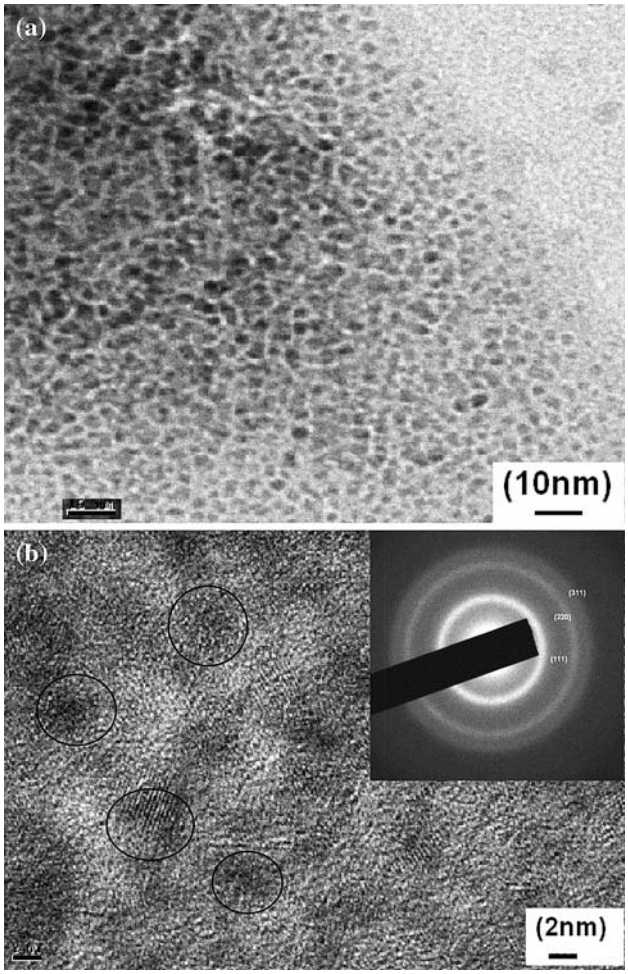

Fig. 2 (**a**) The transmission electron micrograph (TEM) of ZnS:Mn (5%) nanoparticles; (**b**) The high-resolution TEM and the inset shows the selected area diffraction pattern (SAED)

above formula, was found to be ~2.62 nm. No passivating agent has been used in the fabrication of the nanoparticles but still no apparent difference was observed in the XRD peak shape and broadening of ZnS nanoparticles even after two weeks of the fabrication. This suggests that no agglomeration of the particles has taken place.

Figure 2a shows the transmission electron micrograph (TEM) of ZnS:Mn (5%) nanoparticles. The diameters of most of these particles lie in the range of 3–5 nm. This can also be seen from the high-resolution transmission electron micrograph (HRTEM) in Fig. 2b. These results are nearly in accordance with those of the X-ray diffraction analysis. The selected area diffraction pattern presented in the inset of Fig. 2b shows crystallinity of the fabricated nanoparticles. The dominant diffraction patterns in the micrograph are indexed as (111), (220), and (311) planes of the cubical ZnS. Chemical precipitation is widely used for the preparation of colloidal nanoparticles. In the method described above, we used the following exchange/replacement reactions:

$$Zn(CH_3COO)_2 \leftrightarrow Zn^{2+} + 2CH_3COO^- \quad (2)$$

$$Zn^{2+} + Na_2S \leftrightarrow ZnS + 2Na^+ \quad (3)$$

Zn^{2+} ions were reacted with a sulphide (S^{2-}) source, i.e., Na_2S. ZnS forms instantaneously at a certain pH value. The equilibrium of Eq. 2 lies far on the right side because of the high solvation energy in water. The driving force for the reaction (3) is the formation of strong ZnS bonds. The ZnS particles nucleate by consuming more Zn^{2+} and S^{2-} ions from the solution, which can be explained on the basis of Ostwald ripening [14]. Due to high surface energy of the particles, acetate (Ac^-) and sulphur (S^{2-}) anions accumulate around the ZnS particles, thereby attracting the Zn^{2+}, Na^+, and Mn^{2+} cations. Zn^{2+} and Mn^{2+} react with S^{2-} get incorporated into the crystal lattice whereas Na^+ ions accumulate to form the stern layer over ZnS nanoparticles, attracting Ac^- ions to form a diffuse layer over it. In this way, the particle growth is completely stopped [15].

Figure 3 shows the FTIR spectra of the synthesized nanoparticles, confirming the interaction of acetate anions derived from the starting zinc acetate, with the ZnS nanoparticles. The bands at 1404 cm^{-1} and 1558 cm^{-1} can be assigned to the symmetric and asymmetric stretching of COO^-, respectively [16]. The broad band at 3366 cm^{-1} is due to O–H stretching and band at 929 cm^{-1} is due to O–H out of plane bending whereas the band having moderate intensity at 1339 cm^{-1}, may be due to the in-plane C–O–H bending [17]. A strong intensity band at 1019 cm^{-1} may be due to S–O–C stretching. The stretching vibrations assigned to the C–S linkage occur in the region of 700–600 cm^{-1} and the weak S–S stretching vibration falls between 500 and 400 cm^{-1}. Thus, the acetate ions are acting as inbuilt surfactants to control the size of the ZnS nanoparticles.

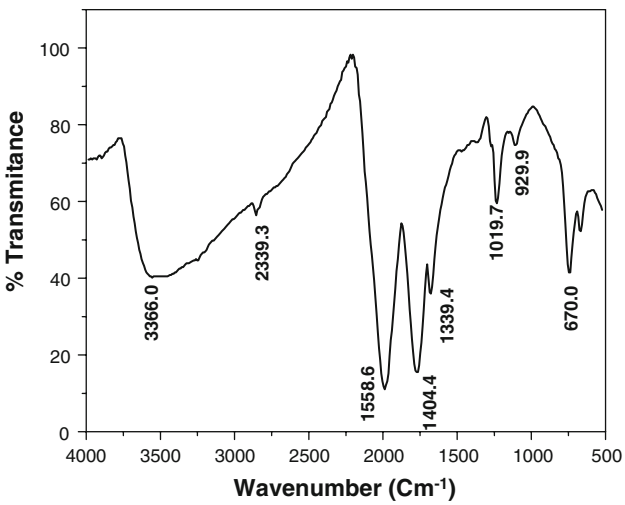

Fig. 3 FTIR spectra of ZnS nanoparticles having a layer of acetate ions adhered to its surface

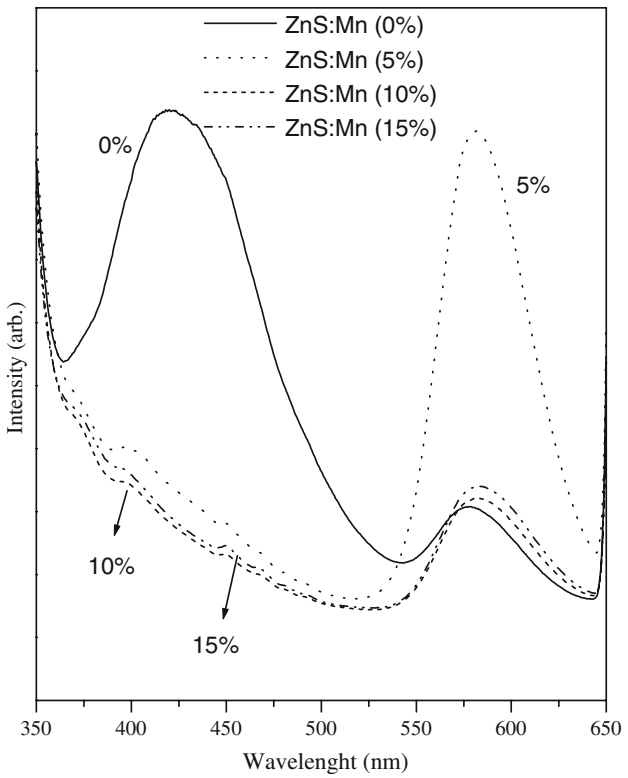

Fig. 4 Room-temperature PL spectra of the ZnS:Mn nanoparticles

Room-temperature photoluminescence spectra of the ZnS:Mn nanoparticles measured with a 335 nm excitation wavelength are shown in Fig. 4. Photoluminescence spectra for the undoped ZnS nanoparticles showed two emission bands, one blue emission at ~420 nm and another yellowish green band at 575 nm. The blue emission band was associated with the recombination of free charge carriers at defect sites, possibly at the surface of nanostructures [18, 19]. The yellowish green band at ~575 nm was most likely due to the self-activated defect centres formed by the zinc vacancy inside the lattice [20, 21]. The orange emission around 582 nm can be attributed to the $^4T_1$–$^6A_1$ transition of the Mn^{2+} impurity. The characteristics of the Mn^{2+} impurity are almost identical to the emission observed for Mn^{2+} in bulk ZnS [22]. The intensity of the orange emission (582 nm) first increased and then decreased with the increase of Mn concentrations. Emission intensity is much higher for 5% incorporation as compared to 10% and 15% doping. This effect might be due to concentration quenching, due to which the increased availability of the dopant ion increases the number of energy transfers between the initially absorbing impurity ions, to another identical ion instead of immediately resulting in radiation (luminescence). After a number of such processes, a transfer to a quenching site (e.g., a defect) may become involved, thus further decreasing the radiative process. This explains that the increase in Mn impurity

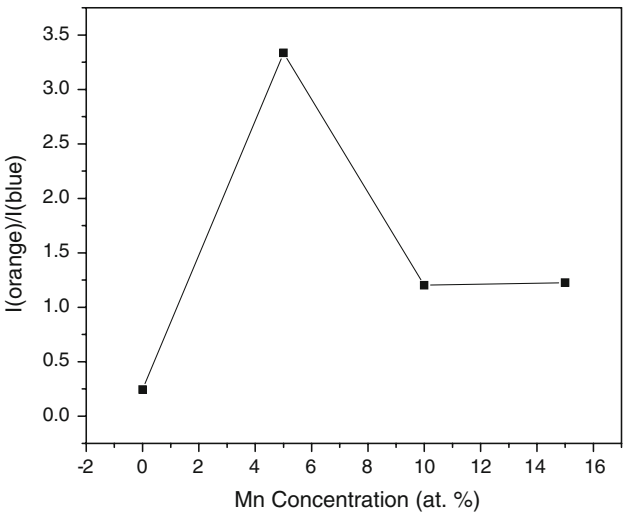

Fig. 5 Actual intensity ratio of the orange to blue emissions vs. at.% of Mn

concentration above a certain value could lead to a reduction in PL intensity [23]. This is also clear from Fig. 5, which shows that as Mn concentration increases to 5%, there is an increase in orange emission intensity as compared to blue emission. But the further increase in Mn concentration leads to gradual decrease in the orange emission intensity. The yellowish-green emission (575 nm) disappeared on addition of Mn to the ZnS nanoparticles; this indicates that its origin could be zinc-vacancy related defect states. The addition of the Mn^{2+} ion could have filled the Zn vacancy sites, resulting in the reduction of the intensity of this peak, due to quenching of self-activated centres. It was also observed that PL peak position (582 nm) is independent of the Mn concentration.

Figure 6 shows the optical absorption spectra of the ZnS:Mn nanoparticles. The absorption coefficient (α) was

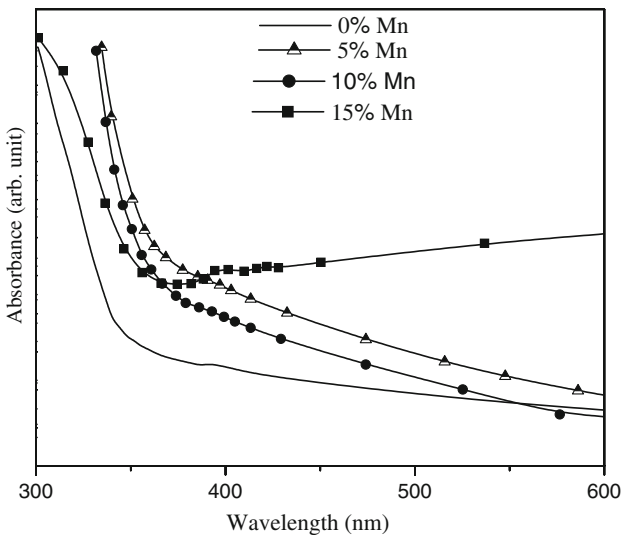

Fig. 6 Plot of absorbance vs. wavelength of ZnS:Mn nanoparticles

determined from the absorbance vs. wavelength (λ) traces recorded for the Mn-doped and undoped ZnS nanoparticles. The optical band gap (E_g) in a semiconductor is determined by assuming the nature of transition (m) and plotting $(\alpha h\nu)^{1/m}$ vs. $h\nu$, where m represents the nature of transition. Now, m may have different values, such as 1/2, 2, 3/2, or 3 for allowed direct, allowed indirect, forbidden direct, and forbidden indirect transitions, respectively [24]. For allowed direct transition $(\alpha h\nu)^2$ vs. $h\nu$ was plotted and the linear portion of it was extrapolated to $\alpha = 0$ value to obtain the corresponding band gap (E_g) (Fig. 7). For undoped ZnS nanoparticles, the band gap has been calculated to be 3.88 eV, which indicates a blue shift as compared to the band gap of bulk ZnS (3.66 eV), indicating the quantum confinement in the ZnS nanocrystallites. It may also be noticed that the band gap values of Mn-doped ZnS nanoparticles has reduced, which is due to the Mn related levels introduced in the host lattice. This can also be confirmed from the trap depth values as obtained from the time-resolved PL spectra discussed ahead (Table 1).

Time-resolved photoluminescence provides an effective nondestructive technique for studying the dynamics of

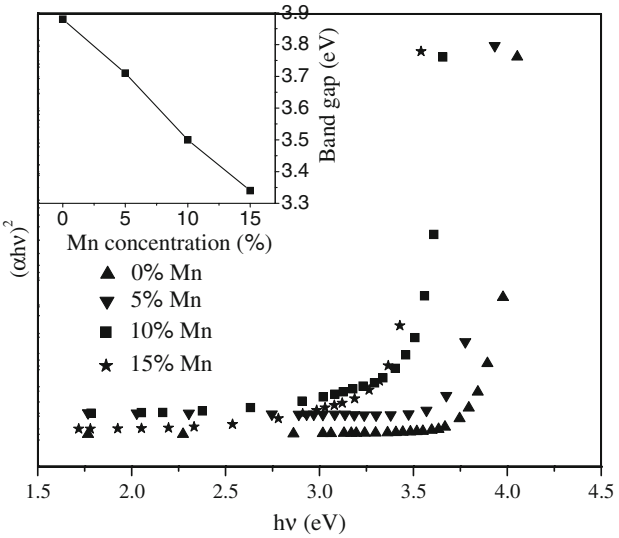

Fig. 7 Plot of $(\alpha h\nu)^2$ vs. $h\nu$ for the ZnS:Mn nanoparticles with inset showing the variation of band gap with Mn concentration

Table 1 Band gap values of ZnS:Mn nanoparticles calculated from optical absorption spectra

S. No.	Sample	Band gap (eV)
1	ZnS (Bulk)	3.66
2	ZnS:Mn (0%)	3.88
3	ZnS:Mn (5%)	3.71
4	ZnS:Mn (10%)	3.50
5	ZnS:Mn (15%)	3.34

impurities and lattice defects in semiconductors [20]. The intensity of the luminescent radiation, at time t, is given as

$$I = I_o e^{-pt} \tag{4}$$

where I_o is the intensity of radiation at cut-off position, the constant $p = 1/\tau$ is the transition probability of the corresponding radiative transition, and τ is the lifetime of the excited state. Figure 8a and b shows the intensity vs. time graph recorded as per the time-resolved photoluminescence spectra for ZnS:Mn. The decay curves can be peeled-off into three components by the peeling-off method of Bube. The results of decay curves can be expressed as:

$$I = I_{o1}\exp(-p_1 t) + I_{o2}\exp(-p_2 t) + I_{o3}\exp(-p_3 t) + \cdots \tag{5}$$

where p_1, p_2, and p_3 are the transition probabilities. I_{o1}, I_{o2}, and I_{o3} are the intensities at the cut-off position for three probability values. In the present investigation only three components have been taken because further components were having the life times in the order of few seconds. The dopant has introduced multiple trapping levels at different depths below the conduction band in the host material in ZnS. Table 2 shows the excited state lifetime values for ZnS:Mn nanoparticles, recorded at room temperature, for blue emission (~420 nm) and for manganese-related orange emission (~585 nm).

The levels, introduced by Mn in ZnS nanophosphors, are $^4T_1$–$^6A_1$, which is a forbidden transition by spin selection rules and its probability is very low which gives long lifetimes, as observed for orange emission as compared to the blue emission in Table 2. As the concentration of Mn is increasing the life times are reducing (Table 2) from 31.51 μs (for 5 at.%) to 15.86 μs (for 15 at.%). This is due to the smaller lifetimes of the excited state of interacting pairs as compared to a single Mn^{2+} centre [25]. With the increase in the concentration of Mn impurity, the number of such interacting pairs have increased (leading to concentration quenching), causing the decrease in excited state lifetimes.

As mentioned in Table 3, the value of trap depth, E, has been calculated using the Boltzmann's equation [26]:

$$p = S\,e^{-E/kT} \tag{6}$$

where S is the escape frequency factor (~10^9 s^{-1}), k is the Boltzmann's constant, and T is the absolute temperature. The distribution of traps in the energy band gap of the nanoparticles has been studied using the following equation:

$$I = I_o t^{-b} \tag{7}$$

where b is the decay constant. The value of decay constant explains the distribution of the trapping states introduced by the dopant within the band gap of the phosphor. If the

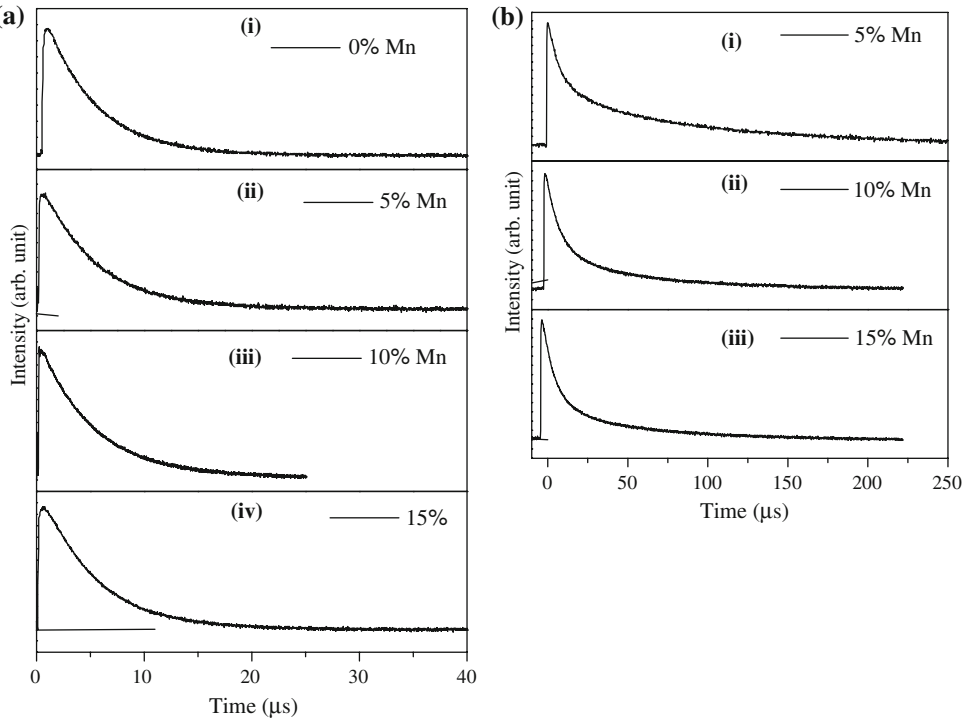

Fig. 8 (**a**) Hyperbolic decay curves for ZnS:Mn nanoparticles at 420 nm; (**b**) Hyperbolic decay curves for ZnS:Mn nanoparticles at 585 nm

Table 2 Excited state lifetime values for ZnS:Mn nanophosphors recorded at room temperature

S. No.	Sample	Excited state lifetime values (μs) for blue emission (420 nm)			Excited state lifetime values (μs) for orange emission (585 nm)		
		τ_1	τ_2	τ_3	τ'_1	τ'_2	τ'_3
1	ZnS:Mn (0%)	6.89	13.22	55.08	–	–	–
2	ZnS:Mn (5%)	7.10	14.28	67.94	31.51	126.66	318.95
3	ZnS:Mn (10%)	7.58	19.12	142.88	26.52	116.47	462.64
4	ZnS:Mn (15%)	8.04	27.43	428.47	15.86	42.25	135.31

Table 3 Trap depth values and decay constant for ZnS:Mn nanophosphors recorded at room temperature

S. No.	Sample	Trap depth values (eV for orange emission (585 nm)			Decay constant
		E_1	E_2	E_3	
1	ZnS:Mn (5%)	0.2683	0.3043	0.3282	1.0969
2	ZnS:Mn (10%)	0.2638	0.3021	0.3379	1.4655
3	ZnS:Mn (15%)	0.2505	0.2759	0.3060	1.9559

value of decay constant is unity, the traps introduced by the impurity are uniformly distributed within the band gap of the nanoparticles. Otherwise there will be nonuniform distribution of the traps. The trap depth is maximum (0.2683 eV) for ZnS doped with 5% of Mn and minimum (0.2505 eV) for 15% Mn doping. This shows that as the concentration of Mn has increased from 5% to 15%, the levels introduced by Mn impurity have become shallow. The decay constant values show that the distribution of the traps within the energy band gap of phosphors is nonuniform, and this nonuniformity has increased with the increase in the dopant concentration.

Conclusion

In summary, we have fabricated ZnS nanoparticles ($\sim$3 nm) doped with various concentrations of Mn without using any external capping agent. However, the FTIR spectra confirmed that the acetate ions, derived from zinc

acetate, have been found to act as in-built surfactants so as to control the particle size. The cubic (zinc blende) structure of the fabricated nanoparticles has been observed using XRD studies. UV–visible absorption spectra have been studied. Quantum confinement was observed, as a blue shift has been observed from the optical band gap values for ZnS nanoparticles, whereas subsequent increase in band gap values on addition of Mn as a dopant was due to the levels introduced by the dopant in the host material. This has also been confirmed from the trap depth values (varying from 0.3379 eV to 0.2505 eV), calculated by time-resolved PL decay curves. Concentration quenching has reduced the PL intensity for higher concentration of Mn impurity and has also decreased the life times of the excited states.

Acknowledgement We acknowledge Defence Research and Development Organisation (DRDO), Government of India, for their generous funding for the research work vide their letter No. ERIP/ER/0504321/M/01/855 dated 16th December 2005.

References

1. Bhargava RN (1997) J Lumin 72–74:46. doi:10.1016/S0022-2313(96)00162-7
2. Bhargava RN (1996) J Lumin 70:85. doi:10.1016/0022-2313(96)00046-4
3. Zhao Y, Zhang Y, Zhu H, Hadjipanayis GC, Xiao JQ (2004) J Am Chem Soc 126:6874. doi:10.1021/ja048650g
4. Lu SW, Lee BI, Wang ZL, Tong W, Wagner BK, Park W et al (2001) J Lumin 92:73. doi:10.1016/S0022-2313(00)00238-6
5. Hu JT, Li LS, Yang WD, Manna L, Wang LW, Alivisatos AP (2001) Science 292:2060. doi:10.1126/science.1060810
6. Cruz AB, Shen Q, Toyoda T (2005) Mater Sci Eng C 25:761. doi:10.1016/j.msec.2005.06.022
7. Denzler D, Olschewski M, Sattler K (1998) J Appl Phys 84:2841. doi:10.1063/1.368425
8. Chen W, Sammynaiken R, Huang Y, Malm JO, Wallenberg R, Bovin JO et al (2001) J Appl Phys 89:1120. doi:10.1063/1.1332795
9. Kubo T, Isobe T, Sena M (2002) J Lumin 99:39. doi:10.1016/S0022-2313(02)00296-X
10. Lacomi F (2003) Surf Sci 532:816. doi:10.1016/S0039-6028(03)00446-1
11. Yuan H, Xie S, Liu D, Yan X, Zhou Z, Ci L (2003) J Cryst Growth 258:225. doi:10.1016/S0022-0248(03)01502-1
12. Kim D, Min K, Lee J, Park JH, Chun JH (2006) Mater Sci Eng B 131:13. doi:10.1016/j.mseb.2005.11.005
13. Cullity BD (1956) Element of X-ray diffraction, 2nd edn. Addison-Wesley, New York, p 99
14. Yao JH, Elder KR, Guo H, Grant M (1993) Phys Rev B 47:14110. doi:10.1103/PhysRevB.47.14110
15. Warad HC, Gosh SC, Hemtanon B, Thanochayonont C, Dutta J (2005) Sci Technol Adv Mater 6:296
16. Zou X, Ying E, Dong S (2006) Nanotechnology 17:4758. doi:10.1088/0957-4484/17/18/038
17. Silverstein RM, Clayton Bassler G, Morrill TC (1991) Spectrometric identification of organic compounds, 5th edn. Wiley, New York, pp 91–164
18. Bol AA, Meijerink A (1998) Phys Rev B 58:R15997. doi:10.1103/PhysRevB.58.R15997
19. Kar S, Chaudhari S (2005) J Phys Chem B 109:3298. doi:10.1021/jp045817j
20. Falcony C, Garcia M, Ortiz A, Zlonso JC (1992) J Appl Phys 72:1525. doi:10.1063/1.351720
21. Samelson H, Lempicki A (1962) Phys Rev 125:901. doi:10.1103/PhysRev.125.901
22. Bhatti HS, Sharma R, Verma NK (2005) Parmana 65:541. doi:10.1007/BF02704213
23. Cruz AB, Shen Q, Toyoda T (2005) Jpn J Appl Phys 44:4354. doi:10.1143/JJAP.44.4354
24. Bhattacharyya D, Chaudhari S, Pal AK (1992) Vacuum 43:313. doi:10.1016/0042-207X(92)90163-Q
25. Vlasenko NA, Zynio SA, Kopytiko Y (1975) Phys Stat Solidi a 29:671
26. Bube RH (1950) Phys Rev 80:655. doi:10.1103/PhysRev.80.655